

Malignant thyroid lump multi classification by TIRADS using DBA with transfer learning

Mayuresh B. Gulame¹, Vaibhav V. Dixit²

¹Department of Electronics and Telecommunication, G. H. Rasoni College of Engineering and Management, Savitribai Phule Pune University, Pune, India

²Department of Electronics and Telecommunication, Rasiklal M. Dhariwal Sinhgad Technical Institutes Campus 11/1, Maharashtra, India

Article Info

Article history:

Received Feb 9, 2024

Revised Mar 6, 2024

Accepted Mar 28, 2024

Keywords:

Deep learning

Thyroid nodules

TIRADS score

Transfer learning

U Net segmentation

ABSTRACT

Thyroid diseases have developed into significant illnesses in recent decades. These diseases affect the thyroid glands and are caused by elevated thyroid hormone levels or infections in the thyroid organs. It is challenging to resolve thyroid diagnosis using conventional parametric and nonparametric statistical techniques since it can be viewed as a classification problem. However, there are certain barriers in the manner of obtaining both efficacy and accuracy in thyroid nodule diagnosis. Deep learning (DL) and machine learning (ML) models have emerged as useful instruments for the diagnosis of sickness in the modern era. For the purpose of diagnosing and classifying thyroid diseases, this research introduces a novel deep belief network (DBF) with transfer learning, known as DBNTL. In this study, the pre-processed image was first pre-processed using a conventional multiresolution bilateral technique, and then it was subjected to a novel segmentation technique called fusion pooling integrated U-net segmentation. The DBN with transfer learning model is used to classify and grade malignant thyroid nodules in compliance with thyroid imaging-reporting-and-data-system (TIRADS) guidelines. In this model, the model's weights are obtained by transfer learning. A major metric for evaluating the efficacy of biological image processing applications, good sensitivity and specificity (97.28 and 97.22, respectively) were obtained for the recommended modes.

This is an open access article under the [CC BY-SA](https://creativecommons.org/licenses/by-sa/4.0/) license.



Corresponding Author:

Mayuresh B. Gulame

Department of Electronics and Telecommunication, G. H. Rasoni College of Engineering and management Savitribai Phule Pune University

New Gat No. 1200, Domkhel Road, Wagholi, Pune 412207, Maharashtra State, India

Email: mayuresh2103@gmail.com

1. INTRODUCTION

The main Globally, the dominance of thyroid lumps has stayed rising annually due to rising life pressure. It is now among the most significant illnesses and poses a risk to public health. Consequently, it is critical to diagnose thyroid nodules as soon as possible. Thyroid nodule diagnosis is mostly achieved by aspiration biopsy, computed tomography (CT) scanning, ultrasound scanning, and pathological investigation. Nuclear scanning, which is costly and dangerous to people, is necessary for CT exams. Although pathological inspection and needle biopsy are more often employed and trustworthy techniques, they both cause significant damage to thyroid tissue. They also have a laborious diagnosing process, which uses up more medical resources. The most prevalent imaging technique used to diagnose thyroid disorders is now ultrasound. Its benefits include little cost, rapidity, non-invasiveness, minimalism, and remarkable

reproducibility. Medical professionals typically rely on extremely subjective and readily influenced clinical experience to determine what is benign and malignant. It is therefore becoming more and more critical to be able to recognise and diagnose the pathology of ultrasound-identified thyroid nodules quickly and properly [1].

Solid, cystic, or mixed lesions can all be seen on ultrasounds of nodules. Malignancy is quite likely in single solid nodules. Whereas pure cystic nodules have a lower risk of malignancy, mixed nodules are still susceptible to it. Ten percent of calcified nodules have the potential to be cancer. The score from the thyroid imaging-reporting-and-data-system (TIRADS) [2] is utilized to categorized thyroid nodules. Founded on features of ultrasonography, TIRADS is a standardised thyroid risk classification approach for thyroid lesions. The threat of cancer, which is based on the quantity of suspicious ultrasonography characteristics, is the foundation of TIRADS classifications. TIRADS-2, TIRADS-3, TIRADS-4a, TIRADS-4b TIRADS-4c, in addition TIRADS-5 are the categorisations of TIRADS-related disorders.

Computer-aided design (CAD) systems are designed to help radiologists quickly assess information from medical imaging for accurate diagnosis and detection, as well as to help interpret ultrasound pictures of thyroid nodules. As such, to give sufficient information for an accurate assessment of thyroid nodules, CAD [3] systems with TIRADS score that are capable of detecting and classifying thyroid nodules into several stages of malignancy are required. Multi-class picture categorization is improved by recent developments in deep learning. So, in this paper we suggested unique way for ordering of thyroid lumps.

The structure and contribution of the paper is as follows:

- Fusion pooling integrated U-Net segmentation (FPIU-Net) of thyroid nodules is shown together with the pre-processing.
- Transfer learning is used to build weights in the model by sending these extracted features to the suggested DBNTL technique.
- Section 3 then provides a description of the experimental outcomes. The last section of the presentation is the conclusions.

2. LITERATURE SURVEY

Chu *et al.* [4] suggested an ultrasound deep network segmentation method for the diagnosis of thyroid nodules in 2021. The results of the ultrasonography thyroid nodules were incomplete; therefore, during the diagnosis process, the segmentation output and the doctor's prepared data were combined. The CNN-based U-net model is necessary for this kind of nodule segmentation. As a result, the performance of the proposed model in improving the accuracy of thyroid nodule segmentation is well-acted upon by the U-net model. Table 1 summarized work done till now in thyroid lump classification. A novel multimodal domain adaptation technique known as SCGAN was identified in 2022 by [5]. It employed cross-domain mutual coalition of nodule images.

They employed an individual attention strategy for learning through competition between concurrent domains in order to get beyond visual variances among modal data and maintain the domain consistency that defined the retrieved semantic features. DL was proposed as a new diagnostic paradigm in 2023 by Fresilli *et al.* [6]. Localization-classification diagnostics is the diagnostic method employed by the system. The distribution criteria controlling nodule size and nodular aspect ratio were initially established a priori for networks using a multi-scale localization architecture. The placement results were used to construct the overall nodule aspect ratio. A joint-training CNN for the identification of thyroid nodules in ultrasound images was presented by Tang *et al.* [7]. Because Fast R-CNN is so good at detecting natural targets, they adopted it as our foundation. The module's attention mechanism was incorporated to enhance dynamic features in both spatial and channel dimensions, thereby augmenting representational power and mitigating network noise. Furthermore, they employ a novel technique known as joint training annotations, which increases the sensitivity to tiny nodules during training, by using the FFG area encompassing the nodule as an additional spatial prior constraint to label the collection of training data.

Table 1. Summary of thyroid lump classification by artificial intelligence

Source	Classifier	Architecture	Layers	Sensitivity	Specificity	Accuracy	AUC
[8]	ResNet-50	Darknet-19	50.19	93.40%	86.10%	92.60%	0.947%
[9]	Elastic net	Elastic Net	NA	90.07%	94.90%	96.70%	0.954%
[10]	Google net	ANN, SVM	3	99.10%	93.90	98.29%	NA
[11]	Bi-LSTM	Bi-LSTM	3	0.939%	NA	0.8618%	0.9361%
[12]	VGG16, ResNet50	Res-Net50	50	NA	85.20%	0.83%	89.20%

3. METHOD

The Figure 1 shows the proposed method for new segmentation and classification task. Here we have used two types of datasets. The fusion-based segmentation method used followed by preprocessing by boosted winner filter. The segmented image is given for feature extraction using Inception V3+ Google Net method. Lastly classification done with transfer leaning strategy.

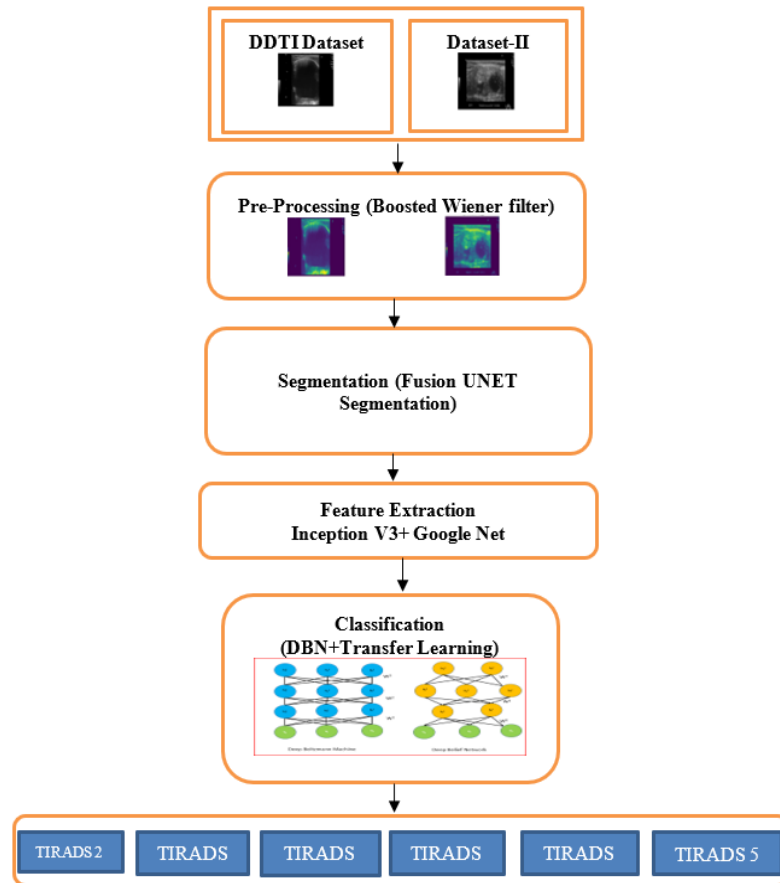


Figure 1. Overall flow of proposed methodology

3.1. Pre-processing

Taking into account the two datasets, digital database of thyroid ultrasound images (DDTI) and Dataset 2 (manually collected), where the input image is represented as Im . Initially, the image Im is pre-processed to provide a denoised image suitable for subsequent processing. A certain amount of noise may occur during the image's capture and transfer, which alters the image's visual effects by causing random spots of light or dark noise. This work uses the multi-resolution bilateral technique to eliminate the undesirable noise from the image [13]. According to this architecture, the input signal is divided into frequency subbands. By applying the bilateral filter to the approximate subband during reconstruction, low frequency noise components are reduced. When compared to a bilateral filter of type single-level, this drop is advantageous to a multiresolution bilateral filter.

This design consists of two primary phases. In the first phase, the bilateral filter's ideal parameter selection is examined, and in the second, the bilateral filter is extended: when using a wavelet filter bank, an image's approximation subband is subjected to the bilateral filter of multiresolution. This concept produces an efficient denoising image framework when combined with wavelet thresholding, which removes noise from the provided medical ultrasound image.

3.2. Fusion pooling integrated U-Net segmentation

The ultrasonic image is first cleaned up by applying a median filter to eliminate paper noise and salt. We use this pre-processed image as input for our segmentation block. This image undergoes use of the

modified U-net segmentation technique [14], [15]. Our innovative segmentation method's flow is illustrated from input image to segmentation in the accompanying Figure 2. In this improved segmentation method instead of using Max-pooling we have considered mixed pooling and mathematical significance of mixed pooling is explained in (1).

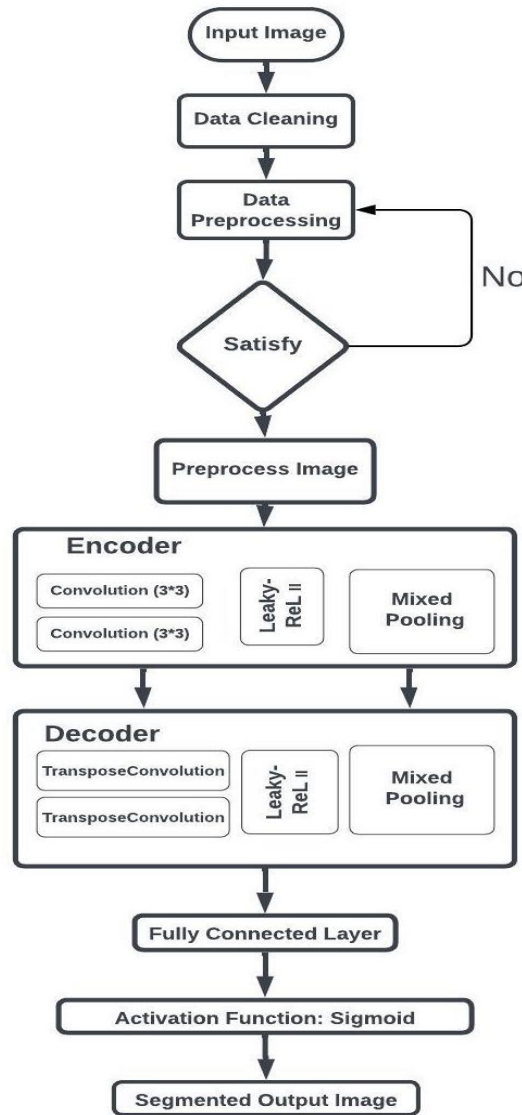


Figure 2. Proposed method for thyroid lump segmentation

Localization tasks are successfully completed by sliding window method on all training datasets. Each pixel is assigned a unique class identification after receiving a local patch. However, there are two main issues with this design. Overall, there is a significant degree of redundancy due to the overlapping patches. Second, it took a long time and a lot of resources to complete the training procedure. The architecture was unusable for many applications because of these features. It is U-Net that resolves these two concerns [16].

A network of encoders is used in the method. In this encoder network, there are four encoder blocks. There are two convolutional layers after a leaky rectified linear unit (ReLU) activation function, each with a 3×3 kernel dimension and appropriate padding. This is fed into a mixed pooling layer using a 2×2 kernel dimension. The mixed pooling layer lowers the learned spatial dimensions and cuts the computational cost of training the model by half. According to the (1), fusion pooling integrated U-Net (FPIU-Net):

$$Fusion\ pooling = \eta \cdot \max_{(a,b) \in A_{i,j}} I_{P_{kab}} + (1 - \eta) \cdot \frac{1}{|A_{i,j}|} \sum_{(a,b) \in A_{i,j}} I_{P_{kab}} \tag{1}$$

where, $I_{P(i,j)}$ is the pixel significance of i -th row and j -th column of image I_p , η signifies arbitrary value in the interval $[0, 1]$, $|A_{i,j}|$ is the pooling area dimension, and m and n are the width and height of the image I_p , correspondingly [17].

The bottleneck layer is located between the networks for encoders and decoders. As can be seen in the diagram up top, this is the bottom layer. It has two convolutional layers and then leaky ReLU. The final feature map representation comes out of the bottleneck. The expanding network is yet another name for the decoder network. Our plan is to up sample our feature maps to the size of our image [18].

This unit is composed of four decoder blocks. Each block starts with a transpose convolution, shown in the image as up-conv, with a 3×3 kernel size. Joining this output to the appropriate encoder block skip layer connection is the process of concatenating. Once twin convolutional layers with a 3×3 kernel size are employed, a leaky ReLU-activation utility is operational. U-Net can be enhanced by combining multi-scale feature information. The feature map data from the feature withdrawal stage is gathered in the up-sampling step. The segmentation experiment's main network structure in this study is a U-Net network as experience indicates that it can function better even with little data sets.

3.3. Enhanced DBNTL classification

The characteristics were then fed into the hybrid classification-based nodule classification model after the feature extraction and data augmentation process for the dataset DDTI. One popular energy-related technique is the restricted Boltzmann machine (RBM). A bipartite graph is considered. The top layer is called the visible layer, while the bottom layer is called the concealed layer. The nodes, also known as random binary parameters, are applied from 0 to 1. The Boltzmann distribution is simultaneously filled by the entire probability distribution (ϑ, h) . In (2) presents the energy function of the RBM technique, which is converted into free energy. In (3) illustrates how the Boltzmann distribution and configured power are used to calculate the created joint probability distribution [19].

For example, in (4) and (5) are conditionally autonomous since no link is established between the nodes in each layer. This means that in (6) and (7) are also conditionally autonomous, which is why h is reached by $p(h|\vartheta)$. Similarly, h achieves ϑ' of the visible layer by extending the parameters to make ϑ and ϑ' symmetric. Here, h is represented as the attributes of the input data [20], [21].

If the visibility layer ϑ is supplied as per (8), the probability associated with the j th node of the hidden layer is between 1 and 0. Similarly, if the hidden layer is represented in (9), there is a chance that the i th node in the visible layer is 1 or 0. Next, the free energy function is expressed in terms of a set of samples that meet the requirements of an independent and comparable distribution: $D = \{\vartheta_1, \vartheta_2, \vartheta_3, \dots, \vartheta_n\}$. The characteristics $\theta = \{X, a, b\}$ must be learned, and the RBM Log-likelihood gradient. In this case, ϑ and h are defined as visible and concealed unit, respectively. The relationship weight between the visible and hidden layers is represented by W , the bias of the visible layer's neurons is shown by b' , and the relevant hidden layer bias is shown by c' [22]. The energy calculated by the RBM network is shown as follows from the set of states (ϑ, h) :

$$E(\vartheta, h) = -b'\vartheta - c'\vartheta - h'X\vartheta, \quad (2)$$

$$F(\vartheta, h) = -b'\vartheta - \sum_i \log \sum_{h_i} e^{h_i(c'_{i+X_i}e^{c_i+X_i\vartheta})} \quad (3)$$

the variable of RBM is denoted by $\theta = \{X, b', c'\}$. The joint probability density distribution of (ϑ, h) can be achieved if the parameters are measured in accordance with the energy function:

$$P(\vartheta, h) = \frac{1}{z(\theta)} \exp(-E(\vartheta, h)) \quad (4)$$

$$= \frac{1}{z(\theta)} \prod_{ij} e^{X_{ij}v_i h_j} \prod_i e^{b_{ij}\vartheta_i} \prod_i e^{c_{ij}h_j}$$

wherever the energy total is possible, the normalization factor is defined by (θ) . It is created by categorizing the total energy sum of all possible states and the energy of a given condition as follows:

$$z(\theta) = \sum_{h,\vartheta} \exp(-E(\vartheta, h)), \quad (5)$$

$$p(h|\vartheta) = \prod_i p(h_i|\vartheta), \quad (6)$$

$$p(h|\vartheta) = \prod_i p(\vartheta_j|h), \quad (7)$$

then, possibility of activation of j ih hidden unit is:

$$p(h_i = 1|\vartheta) = \frac{e^{c_i+X_i\vartheta}}{1+e^{c_i+X_i\vartheta}} = \sigma(c_i + X_i\vartheta) \tag{8}$$

the activation probability of the jt^{TM} visible unit is defined as follows: as the architecture of RBM is uniform, the state of the hidden unit is represented and all visible unit activation states are autonomous [23].

$$p(h_i = 1|\vartheta) = \sigma(b_j + X'_j h) \tag{9}$$

In (7) and (8) clearly show that ci and bi are related bias scores.

$$F(\vartheta) = -b'\vartheta - \sum_i(\log(1 + e^{(c_i+X_i\vartheta)})) \tag{10}$$

The accurate in-depth features of real data are achieved by superposing a multilayer RBM, which is known as the DBN. A DBN's structure is implied by Figure 3. Subsequently, the weight is achieved through the utilization of the unsupervised greedy algorithm (GA) [23], [24]. Variables are used to train RBM at the beginning. Subsequently, the GA is applied to achieve the desired weight without supervision. Variables are used to train RBM at the beginning. The variables of the first layer of RBM are then trained layer by layer, with the outcome of the unseen layer serving as input for both the first and second layers of RBM [25], [26]. Furthermore, the resulting hidden layer has been connected to the Softmax regression classification, and the gradient descent (GD) technique is used for fine-tuning (FT). Figure 3 shows the structure of DBL+ Transfer learning.

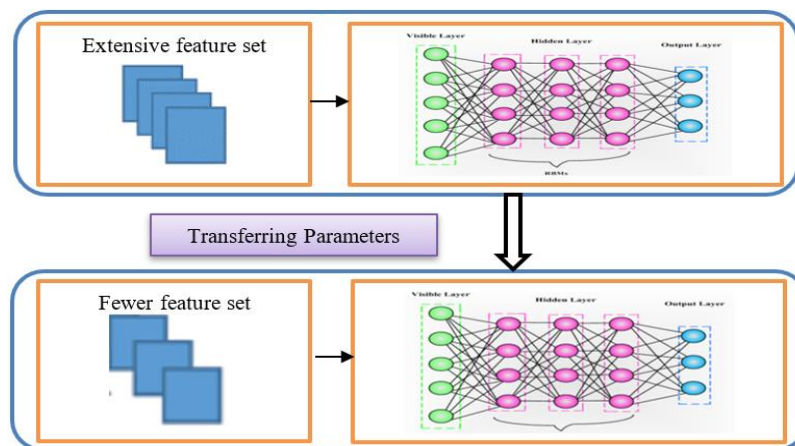


Figure 3. Technique for DBL+transfer learning

4. RESULT AND DISSCUSSION

The new fusion-based segmentation method gives satisfactory output which is input to our proposed classification strategy. The DBNAAF work has been thoroughly addressed for the classification of TIRDAS score based on the examination of other measures. Additionally, the DBNAAF is calculated using the DDTI dataset and dataset2 in conjunction with the deep convolutional neural network (DCNN), you only look once v3 dense multireceptive fields (YOLOV3-DMRF), DBN, bidirectional gated recurrent unit (Bi-GRU), deep maxout, and recurrent neural network (RNN). Our proposed DBNAAF performance is excellent in term of sensitivity, specificity and NPV parameters. Moreover, it not gives good result in binary classification, it also gives good accuracy for multiclass classification.

Table 2 elaborate how our proposed method outperforms satisfactory for all performance metrics. Our proposed method compared with conventional and popular methods with all necessary quality measures. Bi-GRU and DCNN performs well but for all parameter except precision. But our proposed methods give excellent outcome in all parameters.

Figure 4 shows graphical analysis shows how our proposed DBNTL classification technic has good outcome well by comparison with popular conventional methods. DBN and Bi-GRU performs well in accuracy and specificity but sensitivity is not good. But our proposed methodology gives good result in all performance parameters.

Table 2. Performance analysis of proposed DBNTL+FPIU-Net method with conventional methods

Parameter	DBN	RNN	YOLOv3-DMRF	DEEP-MAXOUT	DCNN	Bi-GRU	Proposed DBNTL
Sensitivity	88.94	89.01	86.31	86.70	86.85	87.00	97.28
Specificity	89.63	88.20	86.22	87.49	87.82	87.54	97.22
NPV	89.21	90.23	90.89	90.67	90.34	90.32	98.00
Accuracy	92.23	92.00	90.53	92.83	91.91	91.33	99.64
Precision	85.60	87.65	88.09	86.89	88.26	86.37	97.10

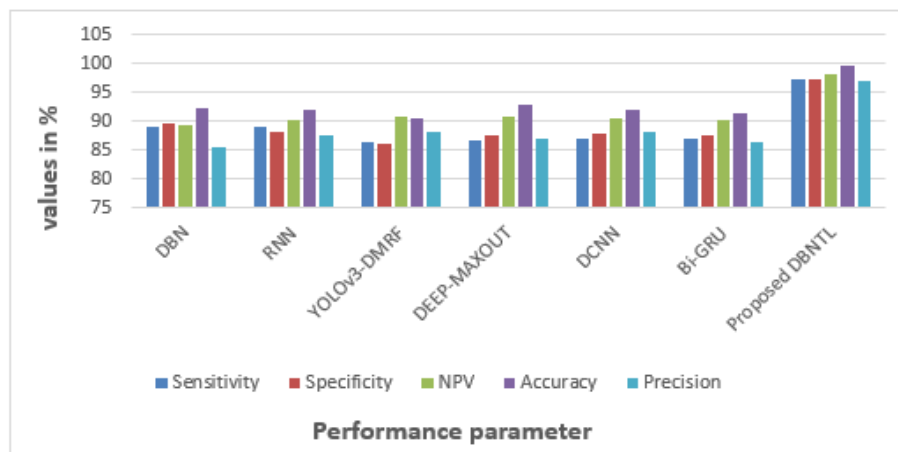


Figure 4. Graphical analysis of all methods with selected quality measures

5. CONCLUSION

In order to identify and categories thyroid nodules, this study presented a novel DBA based deep learning assisted multi-classification method. The bilateral multiresolution technique was used to get a crisp image by removing the speckle noise. The collection of segments was then acquired using segmentation based on FPIU-Net. These segmentate image has been given to proposed DBNTL classifier to classify thyroid nodules. The experimental result shows that our proposed model give good outcome as compared to sate of art methodology. The proposed model got 97.28, 97.22, 98.00, 99.64, 97.10, sensitivity, specificity, NPV, accuracy, precision respectively. Radiologists can avoid misdiagnosis due to overwork by using our proposed CAD approach as a trustworthy second opinion. Moreover, it might provide valuable recommendations for junior radiologists who lack sufficient clinical experience.

REFERENCES

- [1] J. Chi, E. Walia, P. Babyn, J. Wang, G. Groot, and M. Eramian, "Thyroid nodule classification in ultrasound images by fine-tuning deep convolutional neural network," *Journal of Digital Imaging*, vol. 30, no. 4, pp. 477–486, 2017, doi: 10.1007/s10278-017-9997-y.
- [2] T. Rago and P. Vitti, "Risk stratification of thyroid nodules: from ultrasound features to TIRADS," *Cancers*, vol. 14, no. 3, p. 717, Jan. 2022, doi: 10.3390/cancers14030717.
- [3] D. D. Kulkarni and V. V. Dixit, "Automatic emotion detection using electroencephalogram," in *ICCCE 2021*, 2022, pp. 845–851. doi: 10.1007/978-981-16-7985-8_89.
- [4] R. Liu *et al.*, "Diagnostic accuracy of different computer-aided diagnostic systems for malignant and benign thyroid nodules classification in ultrasound images," *Medicine*, vol. 98, no. 29, p. e16227, Jul. 2019, doi: 10.1097/MD.00000000000016227.
- [5] N. Chambara and M. Ying, "The diagnostic efficiency of ultrasound computer-aided diagnosis in differentiating thyroid nodules: a systematic review and narrative synthesis," *Cancers*, vol. 11, no. 11, p. 1759, Nov. 2019, doi: 10.3390/cancers11111759.
- [6] D. Fresilli *et al.*, "Thyroid nodule characterization: how to assess the malignancy risk. update of the literature," *Diagnostics*, vol. 11, no. 8, p. 1374, Jul. 2021, doi: 10.3390/diagnostics11081374.
- [7] F. Tang, J. Ding, L. Wang, and C. Ning, "A novel distant domain transfer learning framework for thyroid image classification," *Neural Processing Letters*, vol. 55, no. 3, pp. 2175–2191, Jun. 2023, doi: 10.1007/s11063-022-10940-4.
- [8] N. Gökmen Inan, O. Kocadağlı, D. Yıldırım, İ. Meşe, and Ö. Kovan, "Multi-class classification of thyroid nodules from automatic segmented ultrasound images: hybrid ResNet based UNet convolutional neural network approach," *Computer Methods and Programs in Biomedicine*, vol. 243, p. 107921, Jan. 2024, doi: 10.1016/j.cmpb.2023.107921.
- [9] P. Qin, K. Wu, Y. Hu, J. Zeng, and X. Chai, "Diagnosis of benign and malignant thyroid nodules using combined conventional ultrasound and ultrasound elasticity imaging," *IEEE Journal of Biomedical and Health Informatics*, vol. 24, no. 4, pp. 1028–1036, Apr. 2020, doi: 10.1109/JBHI.2019.2950994.
- [10] O. Moussa, H. Khachnaoui, R. Guetari, and N. Khelifa, "Thyroid nodules classification and diagnosis in ultrasound images using fine-tuning deep convolutional neural network," *International Journal of Imaging Systems and Technology*, vol. 30, no. 1, pp. 185–195, Mar. 2020, doi: 10.1002/ima.22363.

- [11] M. Wang, Z. Wei, M. Jia, L. Chen, and H. Ji, "Deep learning model for multi-classification of infectious diseases from unstructured electronic medical records," *BMC Medical Informatics and Decision Making*, vol. 22, no. 1, p. 41, Dec. 2022, doi: 10.1186/s12911-022-01776-y.
- [12] Y. Chen, X. Zhang, D. Li, J. Jin, and Y. Shen, "Classification of a small-data-set thyroid nodules based on supplementary feature layer improved VGG16," in *2020 39th Chinese Control Conference (CCC)*, IEEE, Jul. 2020, pp. 7316–7321. doi: 10.23919/CCC50068.2020.9188671.
- [13] Y. Wu, X. Shen, F. Bu, and J. Tian, "Ultrasound image segmentation method for thyroid nodules using aspp fusion features," *IEEE Access*, vol. 8, pp. 172457–172466, 2020, doi: 10.1109/ACCESS.2020.3022249.
- [14] C. Chu, J. Zheng, and Y. Zhou, "Ultrasonic thyroid nodule detection method based on U-Net network," *Computer Methods and Programs in Biomedicine*, vol. 199, p. 105906, Feb. 2021, doi: 10.1016/j.cmpb.2020.105906.
- [15] S. A. A. Kohl *et al.*, "A probabilistic U-net for segmentation of ambiguous images," in *Advances in Neural Information Processing Systems*, 2018, pp. 6965–6975.
- [16] N. Ibtehaz and M. S. Rahman, "MultiResUNet: rethinking the U-Net architecture for multimodal biomedical image segmentation," *Neural Networks*, vol. 121, pp. 74–87, Jan. 2020, doi: 10.1016/j.neunet.2019.08.025.
- [17] Q. Yang *et al.*, "DMU-Net: dual-route mirroring U-Net with mutual learning for malignant thyroid nodule segmentation," *Biomedical Signal Processing and Control*, vol. 77, p. 103805, Aug. 2022, doi: 10.1016/j.bspc.2022.103805.
- [18] A. MEHRNO, R. OKTAŞ, and M. S. ODABAS, "Feature selection of thyroid disease using deep learning: a literature survey," *Black Sea Journal of Engineering and Science*, vol. 3, no. 3, pp. 109–114, Jul. 2020, doi: 10.34248/bsengineering.695904.
- [19] C. Chang, N. Liu, L. Yao, and X. Zhao, "A semi-supervised classification RBM with an improved fMRI representation algorithm," *Computer Methods and Programs in Biomedicine*, vol. 222, p. 106960, Jul. 2022, doi: 10.1016/j.cmpb.2022.106960.
- [20] Y. Pathak, P. K. Shukla, and K. V. Arya, "Deep bidirectional classification model for COVID-19 disease infected patients," *IEEE/ACM Transactions on Computational Biology and Bioinformatics*, vol. 18, no. 4, pp. 1234–1241, Jul. 2021, doi: 10.1109/TCBB.2020.3009859.
- [21] M. Agarwal *et al.*, "Wilson disease tissue classification and characterization using seven artificial intelligence models embedded with 3D optimization paradigm on a weak training brain magnetic resonance imaging datasets: a supercomputer application," *Medical & Biological Engineering & Computing*, vol. 59, no. 3, pp. 511–533, Mar. 2021, doi: 10.1007/s11517-021-02322-0.
- [22] T. Lilo *et al.*, "Raman hyperspectral imaging coupled to three-dimensional discriminant analysis: classification of meningiomas brain tumour grades," *Spectrochimica Acta Part A: Molecular and Biomolecular Spectroscopy*, vol. 273, p. 121018, May 2022, doi: 10.1016/j.saa.2022.121018.
- [23] R. Gautam and M. Sharma, "Prevalence and diagnosis of neurological disorders using different deep learning techniques: a meta-analysis," *Journal of Medical Systems*, vol. 44, no. 2, p. 49, Feb. 2020, doi: 10.1007/s10916-019-1519-7.
- [24] H. Zhou, B. Liu, Y. Liu, Q. Huang, and W. Yan, "Ultrasonic intelligent diagnosis of papillary thyroid carcinoma based on machine learning," *Journal of Healthcare Engineering*, vol. 2022, pp. 1–8, Jan. 2022, doi: 10.1155/2022/6428796.
- [25] M.-H. Wu *et al.*, "Multi-reader multi-case study for performance evaluation of high-risk thyroid ultrasound with computer-aided detection," *Cancers*, vol. 12, no. 2, p. 373, Feb. 2020, doi: 10.3390/cancers12020373.
- [26] V. M. Joshi and R. B. Ghongade, "Subject noncontingent EEG-based emotion detection using deep learning algorithm," in *Advances in Intelligent Systems and Computing*, 2021, pp. 67–75. doi: 10.1007/978-981-16-0171-2_7.

BIOGRAPHIES OF AUTHORS



Mr. Mayuresh B. Gulame    awarded M.E. degree from SPPU in 2013. And pursuing Ph.D. from G.H. Raisoni college Pune. He is working as assistant professor in MIT Art Design and Technology University Pune. He has having 11.5 years of teaching experience. His research areas include biomedical image processing, signal processing, and deep learning. He can be contacted at email: mayuresh2103@gmail.com.



Dr. Vaibhav V. Dixit    received his Ph.D. degree in E&TC Engineering in 2015 from SPPU, Pune, (India). Presently he is working as Principal, RMD Sinhgad School of Engineering and Director of RMD Sinhgad Technical Institutes Campus, Warje, Pune, (India). His research areas include pattern recognition, neural networks and biomedical applications. He has 23 years of teaching and 5 years Industrial experience. He can be contacted at email: vvdixit73@gmail.com.